Special Collection

# Accelerated Electrochemical Investigation of Li Plating Efficiency as Key Parameter for Li Metal Batteries Utilizing a Scanning Droplet Cell

Stefan Dieckhöfer,[a] Wolfgang Schuhmann,*[a] and Edgar Ventosa*[b, c]

*Dedicated to Prof. Marcin Opałło on the occasion of his 65th birthday*

The scanning droplet cell (SDC) allows for automatized electrochemical experiments leading to time-saving and reproducible experimental conditions. Its implementation for non-aqueous battery research is discussed, and the necessary adaptations to be operated inside an Ar-filled glovebox in complete absence of oxygen and moisture are described. Due to the importance of the use of Li metal electrodes for next-generation high-energy batteries, the complex multi-parameter optimisation of the Li plating/stripping processes are investigated by means of the SDC. In particular, the influence of pulsed Li plating protocols on the coulombic efficiency is evaluated. The results clearly show that fine tuning of the parameters of pulsed Li plating protocols, i.e. the relaxation period and Li plating duration, is required to improve Li plating efficiencies at high current densities.

## 1. Introduction

Energy storage has become essential in many aspects of our day to day lives from portable electronics to implementation of energy from renewable sources to electrification of transportation.[1–3] Among the various energy storage technologies, batteries offer distinct advantages, e.g. high energy efficiency, high energy density and moderate cost, which make them very attractive for a range of applications. In particular, Li-ion batteries have experienced a rapid growth in recent years expecting an increase in manufacturing capabilities from $>160\ GW\,h\,yr^{-1}$ in 2020 to $1{,}500\ GW\,h\,yr^{-1}$ in 2030.[4,5] High energy density and long cycle life are the most attracting features of Li-ion batteries. Although improvements in key performance indicators of Li-ion batteries have been achieved over the last decade, this technology is slowly approaching its theoretical limits so that new battery technologies are being pursued to go beyond these limits.[6] These technologies are thus referred to as post Li-ion battery technologies and include, among other, Li-air, Li–S and all-solid-state batteries.[7–9] The use of Li metal as active material for the negative electrode is highly desired for several post-Li-ion battery technologies due to its high specific charge storage capacity (−3.04 V vs SHE, $3860\ mA\,h\,g^{-1}$ and $2061\ mA\,h\,cm^{-3}$)[10] since it would push substantially the energy density of related batteries. However, the failed commercialization of Li metal batteries by Oil back in the late 90's illustrates the risks and challenges that face the use of Li metal in rechargeable batteries.[11,12] The uneven growth of the Li metal film during the plating progress becomes a critical aspect after consecutive cycles leading to the formation of a high surface area Li metal electrode which is extremely reactive. The uneven growth of the Li film results in three major issues.[12–14] *i)* Continuous consumption of Li inventory related to the reconstruction of the protecting solid electrolyte interphase (SEI). *ii)* Li loss related to electrically disconnected Li; and *iii)* safety issues associated with the formation of high-surface area Li-metal electrodes due to its high reactivity. As a consequence, many efforts have been devoted to the development of strategies to prevent or mitigate the roughening of Li metal films upon multiple plating/stripping cycles.[15–18] In fundamental studies addressing this issue, the use of separators in electrochemical cells, in which the two electrodes are pressed on each other separated by a porous separator, hinders investigations of Li growth. Flooded cells, in which the electrodes are physically separated by leaving a space filled with electrolyte, facilitate analysis and interpretation. However, these cell architectures also have setbacks such as time-consuming setup associated with the assembly of these cells, and lack of reproducibility related to the variable distance between the electrodes from one experiment to another.

[a] S. Dieckhöfer, Prof. Dr. W. Schuhmann
Analytical Chemistry – Center for Electrochemical Sciences (CES); Faculty of Chemistry and Biochemistry
Ruhr University Bochum
Universitätstr. 150, D-44780 Bochum, Germany
E-mail: wolfgang.schuhmann@rub.de
[b] Prof. E. Ventosa
Department of Chemistry
University of Burgos
Plaza Misael Bañuelos s/n E-09200 Burgos, Spain
[c] Prof. E. Ventosa
ICCRAM – International Research Center in Critical Raw Materials
University of Burgos
Plaza Misael Bañuelos s/n E-09001 Burgos, Spain
E-mail: eventosa@ubu.es

Supporting information for this article is available on the WWW under https://doi.org/10.1002/celc.202100733

Special Collection *An invited contribution to the Marcin Opałło Festschrift@ELAN_RUB @SchuhmannLab*

The scanning droplet cell (SDC) is an advanced electrochemical device that has been used in other fields of electrochemistry such as electrocatalysis and corrosion.[19–21] The working principle is based on the confinement of the electrolyte together with a reference and a counter electrode inside a miniaturized electrochemical cell, which is the so-called head of the SDC. This head is fixed on a X-, Y-, Z-stepper motor positioner and is pressed onto the sample surface, which acts as working electrode. Only the area in contact with the electrolyte confined by the miniaturised SDC is electrochemically active so that the electrochemical reactions are spatially localized at this specific spot of the sample surface. Automatization of the system allows the SDC to carry out a large number of non-supervised experiments, optimizing resources and minimizing human error. The technique has been particularly beneficial in combination with high-throughput material preparation techniques, such as e.g. for samples prepared by magnetron sputtering, activity-composition relations were elucidated by combining the spatially resolved electrochemical information provided by the SDC with the spatially resolved compositional information provided by EDS-SEM.[22] Recently, our group adapted the SDC to investigate the plating/stripping of zinc for its use in aqueous Zn metal batteries.[23] In this case, each spot on the substrate becomes a new, reproducible, and fresh sample that allows the SDC to accelerate research on Zn plating/stripping processes. The use of aqueous media facilitated the adaptation of the SDC since the systems could operate in open air using conventional accessories, e.g. reference and counter electrodes, aqueous compatible materials, etc.

Here, the necessary adaptations of SDC to be used in non-aqueous post-Li battery research are shown, and applied to investigate the plating efficiency of Li metal in non-aqueous electrolytes inside an Ar-filled glovebox. The manuscript is divided into two sections, namely the adaptation and validation of the individual elements of the SDC to be operational inside an Ar-filled glovebox and the investigation of the influence of pulsed-charging protocols in Li plating efficiency as a case study.

## 2. Results and Discussion

### 2.1. Development and Validation of a SDC System Under Inert Gas Atmosphere

Despite SDC is a well-established electrochemical methodology, its use has been mainly focused on aqueous electrochemical systems in oxygen-containing environments. However, such conditions impede the investigation of high-energy density materials for batteries such as metallic Li due to its instability against moisture and oxygen. Thus, it is necessary to perform a series of adaptations to the SDC to be suitable for the investigation of high-energy battery materials. Such adaptations are not limited to placing the SDC system inside an Ar-filled glovebox, but they include specific connections using feed-throughs, the use of materials compatible with organic solvents, or inserting organic-based reference and counter electrodes into the head of the SDC.

Figure 1 illustrates the connections between the different elements of the SDC located inside and outside the Ar-filled glovebox. The SDC system is composed of 7 elements, namely an electrochemical cell, syringe pump, strain-gauge force sensor, stepper motor driven micrometre screws, potentiostat, stepper motor controller and PC. Due to the lack of humidity inside the glovebox and the higher risk of electrostatic discharge, the potentiostat, stepper motor controller and the PC are placed outside of the glovebox as recommended by manufacturers (e.g. manual for Autolab). All peripheral hardware components except the potentiostat are configured and controlled by means of an in-house programmed software package "Union". The cell body is mounted on a strain-gauge force transducer to provide a quantitative measure of the SDC tip force on the sample surface. Force values that are recorded with a GSV3-USB amplifier serve as feedback signal for automatic SDC approaches with well-defined force limits. A stepper motor controller allows for a three-dimensional positioning of the SDC head with respect to the substrate stage by means of micrometer screws. A syringe pump is connected to the cell body to automatically replace electrolyte prior to a new experiment. Tube connections are made of polyethylene and sealed with flanges. The potentiostat with its device-specific software is coupled to the SDC via a DIO-based trigger in-/

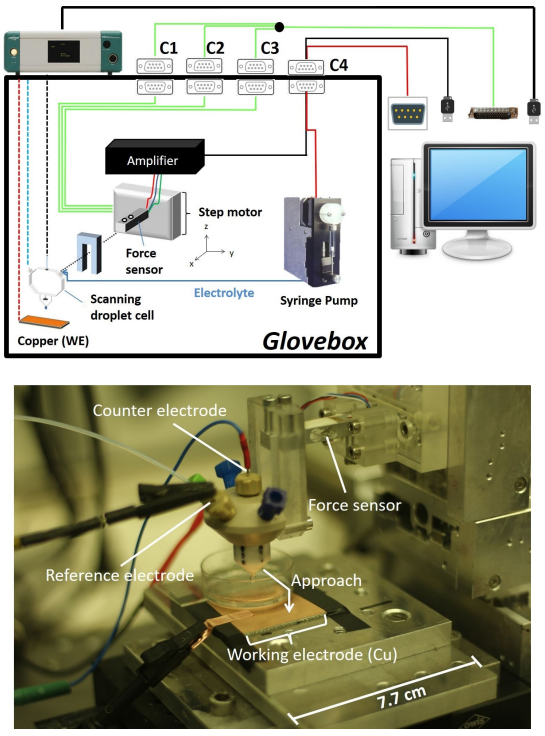


**Figure 1.** Top: Scheme of the SDC inside an argon-filled glovebox coupled to different peripheral devices. All hardware components inside the glovebox are connected to a computer system outside using gas and humidity impermeable passthrough connectors. Bottom: Digital image of the scanning droplet cell set-up installed inside an Ar-filled glovebox. The yellowish tone on the image is originated from the front glass of the glovebox.

output which allows in a simple way to actuate a specific electrochemical measurement sequence of the potentiostat from the main control software. After completion of the electrochemical measurement or measurement sequence controlled by the potentiostat software a reverse DIO-trigger is giving the control back to the main control software. With these automatized sequences of cell rinsing, sample approach and electrochemical testing the variations in electrochemical properties within a predefined array of coordinates become accessible.

Figure 2a shows a scheme of the SDC design capable of operating with non-aqueous electrolytes. The cell head consists of polyether ether ketone (PEEK), a material that is inert towards dissolution in organic media. Both counter (CE) and reference electrode (RE) are gas tight and implemented through channels of the SDC head to place them within the electrolyte inside the tip. By pressing the Teflon orifice on the sample surface with a constant and predefined force, only the defined sample area under the tip is wetted by electrolyte forming a localized 3-electrode cell with a reproducible cell geometry and distances between all electrodes. In this configuration, porous separators are not required. The photograph in Figure 2b illustrates the dimensions of a spot obtained using the SDC that allows addressing large experimental arrays.

Figure 2c displays two exemplary SEM images of spots in which Li plating was previously conducted. Another important aspect for the implementation of the SDC for non-aqueous electrolytes are the reference (RE) and counter (CE) electrodes (Figure 3a). We chose metallic lithium for the RE and CE. In case of the RE, we place a stainless steel canula in the upper part of a channel filled with electrolyte in sufficient distance to the substrate/electrolyte interface, and fix a small piece of Li metal at the end. The canula is further sealed with solder tin to avoid electrolyte evaporation and/or leakage by capillarity. The canula may also be replaced by a thick wire. It should be noted that our RE is not separated from the electrolyte of the main cell.

Attempts to separate the RE using membranes did not result in reliable measurements, so that we decided not to separate it, which is a very common strategy in battery research.[24–26] The stability of the RE potential was evaluated by long-term OCP measurements (Figure 3b). Within a test period of ≈16 h the potential stayed stable within a range of ±2 mV.

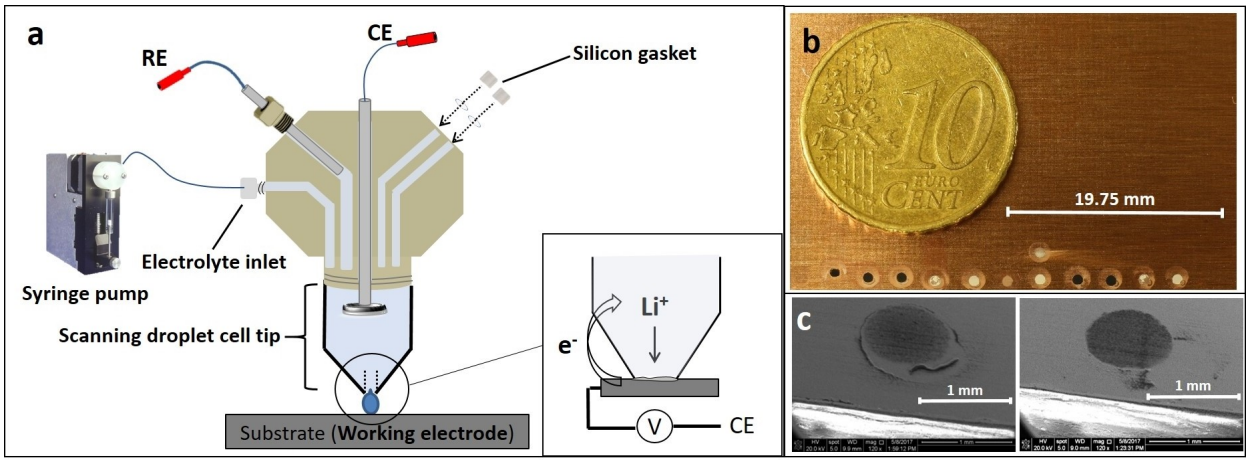


**Figure 2.** a) Illustration of the SDC design for studying the electrochemistry of Li in organic electrolytes. The inset shows how the electroplating of Li only occurs on substrate areas beneath the tip which is wetted with electrolyte. b) Photograph of a Cu substrate on which Li deposits were plated using the SDC as well as a coin of 10-euro-cents for contextualizing the size of the Li deposits. c) SEM images of Li deposits on Cu substrate.

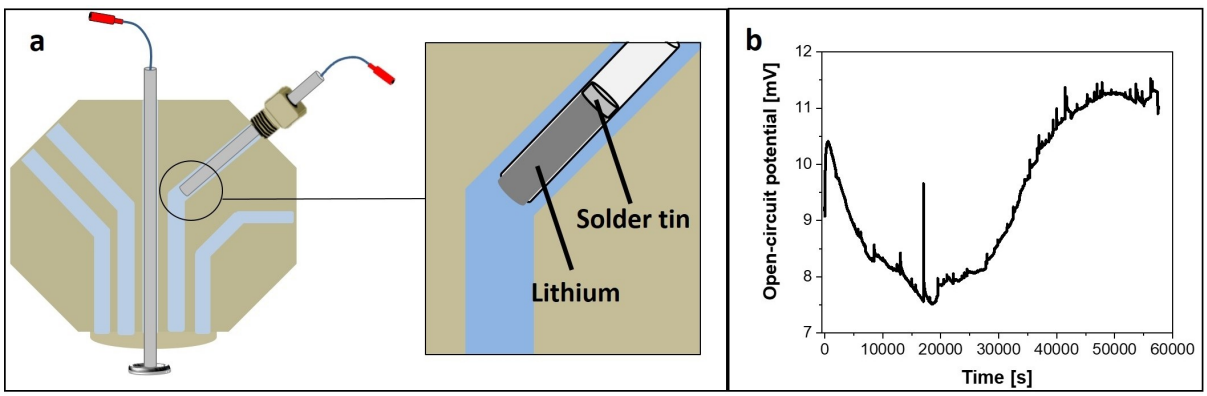


**Figure 3.** a) Schematic illustration of implementation of CE and RE within the SDC head, and b) evolution of the open circuit potential of the home-made Li pseudoreference electrode over time.

Furthermore, the Li metal is located outside the $Li^+$ diffusion field generated by electrochemical reactions at both WE and CE resulting in a constant $Li^+$ concentration close to the RE within the time frame of each experiment. As for the CE, we also chose Li metal since the reversible Li plating/stripping of Li avoids the release of interferences. A disc of Li metal is fixed at the opening of a stainless steel canula to enable electrical contact of the Li metal disc with sealed channel openings (Figure 3a). The canula is also sealed. The dimensions of the Li metal disc (2 mm diameter) for the CE ensures a higher surface area with respect to the confined substrate area (0.5 mm diameter). The central position of the CE is the precondition for a homogeneous and reproducible current line distribution over the wetted WE spot. Proper functioning of the CE is confirmed in Figure 6, in which the evolution of the potential of the WE and CE during galvanostatic measurements at various current densities is displayed.

Finally, the influence of the size of the opening of the miniaturized cell that determines the size of the WE was also evaluated for Li substrates. Larger diameters than 0.5 mm did not provide reliable electrochemical results. Figure S2 shows potential transients from galvanostatic measurements for WE diameters of 0.5 mm and 1 mm, respectively. For 1 mm diameter, small spikes appeared randomly, which is likely due to small leakage of electrolytes when using larger openings. All results on Li substrates shown in this work were hence obtained using a diameter of the SDC opening of 0.5 mm.

Localized cyclic voltammetry experiments on a copper substrate provided evidence for the reversible plating/stripping of Li with the developed SDC. During the initial cathodic scan from +3 V (vs. $Li/Li^+$) to −0.5 V, different redox responses were observed (Figure 4). However, overall the cyclic voltammograms are similar to those reported in literature.[27] The additional small features are assigned to irreversible surface reactions; reduction of copper oxide, oxygen and traces of water, and finally SEI formation on copper (red). The prominent signal at a cathodic overpotential of 110 mV indicates successful plating of Li on copper.

In the anodic backscan a self-crossing of the reduction signal at lower overpotential indicates fast kinetics for Li plating at the same applied potential due to the roughening of the surface and/or the decreased charge transfer resistance after the nucleation phase. The splitting of the anodic Li stripping signal into two peaks at different overpotentials can be rationalized by the presence of different diffusional fields at rough and planar surface features.

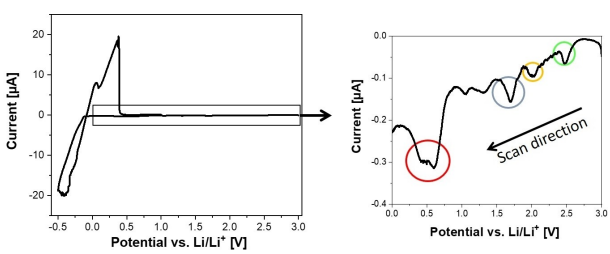


**Figure 4.** Cyclic voltammograms of the SDC on a Cu working electrode at a scan rate of 0.25 mV/s. The inset shows the redox responses of trace components present in the electrochemical microcell.

## 2.2. SDC Investigation of Li Plating Efficiency

Efficient plating of Li is of key importance for the practical implementation of Li metal batteries. Irreversible processes do not only consume Li inventory, but also lead to an increased internal resistance. Consequently, Li plating/stripping processes are an excellent case study to show the beneficial application of the SDC in non-aqueous battery research. Generally, the term Li plating refers to the reduction of $Li^+$ at the negative electrode during battery charging, whereas Li stripping denotes the reverse oxidation of metallic Li during battery discharging. The major challenge regarding the cyclability of Li electrodes at relevant charging rates arises from the fact that Li plating results in high-surface area deposits instead of homogeneous flat films. The initial stage of plating is prone to an inhomogeneous surface coverage with Li nuclei.[15] When Li deposition occurs at a high enough rate, it is governed by a diffusion-limited regime where the further growth of Li seeds is limited by the mass transport of $Li^+$ from the bulk electrolyte. In this situation, sharp surface features benefit from enhanced hemispherical diffusion contrary to planar diffusion towards flat surface regions (Figure 5).[28] Thus, higher plating rates on protruding features trigger a self-accelerated growth of rough structures leading to high-surface area deposits with considerable loss of charge due to SEI formation. Cracks in the SEI due to mechanical stress during the morphological changes further aggravate preferential Li plating and charge consumption by SEI formation.

Several strategies have been proposed in recent years to promote homogeneous growth of Li metal deposits.[15,17] The implementation of pulsed charging protocols in which Li plating is intermittently interrupted was shown to be beneficial to minimize the preferential growth of Li.[29] Consequently, the SDC is here used to study pulse-charging protocols.

The benefit of pulsing is expected to arise from a periodic replenishment of diffusion-depleted $Li^+$ ions during short relaxation intervals without current flow (Figure 5). By this

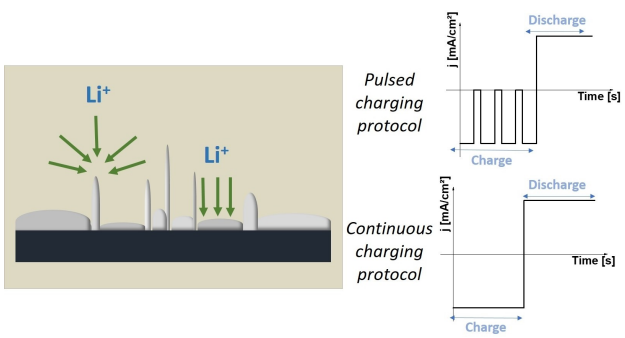


**Figure 5.** Schematic representation of different diffusion fields arising to flat and sharp surface features under diffusion limitation. The exemplary current-time plots illustrate a sequence of Li plating/stripping using pulsed or continuous charging protocols.

means, heterogeneous mass transport phenomena are cancelled out while maintaining sufficiently short charging times. Since smoother Li deposits are expected, we anticipated higher coulombic efficiencies for Li plating/stripping cycles with pulsed charging protocols.

Figure 6 shows the potential profiles obtained using the SDC during typical galvanostatic measurements. The potential of both WE and CE are plotted in black and red lines. This set of measurements was carried out at various current densities for the plating (1 mA cm$^{-2}$, 2 mA cm$^{-2}$, 4 mA cm$^{-2}$ and 8 mA cm$^{-2}$) and constant current density (2 mA cm$^{-2}$) for the stripping process. The SDC systems is able to perform Li plating and stripping within 1–8 mA cm$^{-2}$ range of current densities, and the larger size of the CE ensures that the limiting electrode is the WE since the lower overpotential was recorded at the CE in all measurements. The SDC system can also be programmed to conduct pulsed Li plating protocols followed by continuous Li stripping. Figure 7 shows the evolution of the coulombic efficiencies obtained from the plating/stripping of Li on Cu as a function of the current density for the plating process for continuous protocols and pulsed protocols, which is followed by a stripping step at a constant current density of 2 mA cm$^{-2}$. Deviations from quantitative coulombic efficiencies arise from losses of Li plating charge into side reactions, particularly the SEI formation on continuously evolving Li/electrolyte interphases during Li deposition. In both continuous and pulsed plating protocols, the coulombic efficiency remained constant at *ca.* 80–83 %, and rapidly decreased when current densities above 2 mA cm$^{-2}$ were applied. The higher coulombic efficiency at lower current densities is due to the diffusion-limited plating conditions that modulates the diffusion fields around Li growth centres. At higher current densities, the mass transport is not sufficient for homogeneous growth promoting the growth of dendrite-like spots since mass transport at these sharp objects is enhanced with respect to smooth areas. Regarding the pulsed protocol, there were no significant improvements in coulombic efficiency at lower current densities ($\leq$ 2 mA cm$^{-2}$) for pulse plating protocols with respect to continuous protocols. At 4 mA cm$^{-2}$, pulsed protocols resulted in enhanced efficiency with respect to continuous protocols since mass transport at higher current density becomes an issue. However, similar efficiencies were obtained for pulsed and continuous protocols at 8 mA cm$^{-2}$. Either the pulsed protocols do not have any effect on the coulombic efficiency of Li plating at high current densities or the applied pulsed conditions are not optimal at this current density. Hence, exploring the latter option becomes an interesting case study for the SDC system.

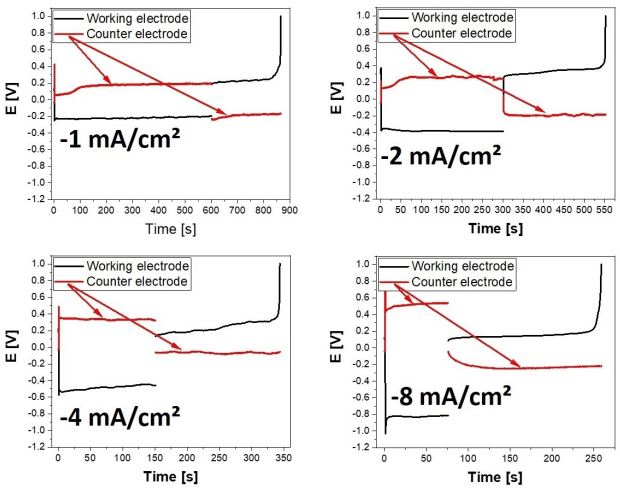


**Figure 6.** Potential transients of working and counter electrode during experimental sequences of Li plating/stripping on copper. Plating current densities are indicated in the plots. Li stripping was constantly performed at + 2 mA/cm$^2$ until the cut-off of + 1 V (vs. Li/Li$^+$) was reached.

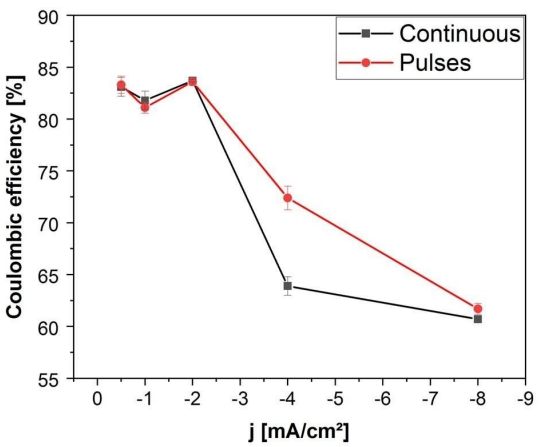


**Figure 7.** Evolution of the coulombic efficiency at various current densities for Li plating (maintaining the current density for the stripping step constant at 2 mA cm$^{-2}$ for continuous plating protocols and pulsed protocols.

Two main parameters of the pulsed protocols were investigated: *i)* duration of the resting period to replenish the concentration of Li-ions in front of the surface, and *ii)* duration of the applied current pulse for Li plating. Obviously, homogeneous and efficient deposition of Li would benefit from shorter plating pulses and longer resting periods, but one also needs to consider the overall duration of the Li plating step (charging time, also referred to as C-rate), which should be as short as possible.

The most demanding conditions, i. e. high current density of 8 mA cm$^{-2}$ for Li plating, were selected to investigate the influence of the parameters of pulsed plating protocols. Figure 8a shows the potential profiles during the stripping step at 2 mA cm$^{-2}$ for Li deposits plated using a constant relaxation time of 0.5 s, while varying the duration of the plating pulse of 8 mA cm$^{-2}$ from 0.125 s to 1 s, together with a table with the resulting coulombic efficiencies. Note that potential profiles are shown separated (Figure S1) to facilitate the interpretation of results. Two main conclusions are drawn from this set of experiments. First, the shorter the plating pulse, the higher the coulombic efficiency (table in Figure 8a). Secondly, the effectiveness in plating of a homogeneous Li film can be evaluated from the potential profiles of the stripping step. In all potential profiles shown in Figure 8, two distinct potential plateaus are observed, which were already previously correlated with the morphology of the surface of the Li electrode.[30] The appearance of the two stripping potential plateaus at a given current

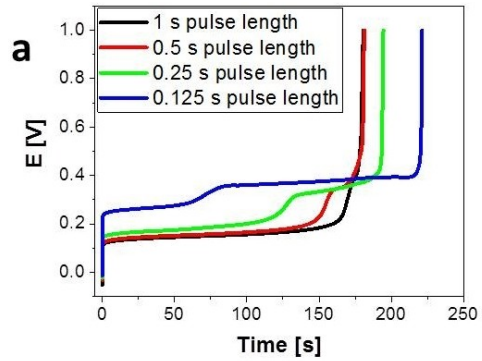


*Pulse duration variation at a fixed relaxation time of 0.5 s*

| Pulse duration $t$ / s | Coulombic Efficiency / % |
|---|---|
| 1 | 54 |
| 0.5 | 61 |
| 0.25 | 65 |
| 0.125 | 73 |

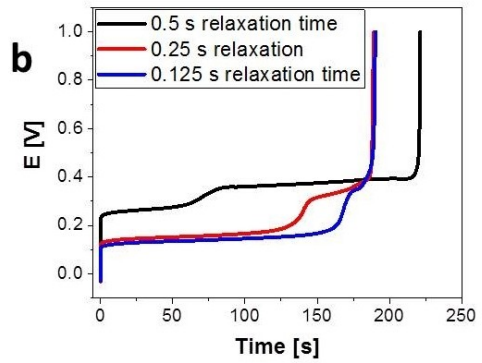


*Relaxation time variation at fixed pulse duration of 0.125*

| Pulse duration $t$ / s | Coulombic Efficiency / % |
|---|---|
| 0.5 | 73 |
| 0.25 | 62 |
| 0.125 | 64 |

**Figure 8.** Potential transients and coulombic efficiencies resulting from: a) variation of the duration the plating pulses (−8 mA/cm$^2$) for a constant duration of the relaxation pulses (0.5 s), b) variation of duration of the relaxation pulses for a constant duration of the plating pulses (0.125 s). All potentials are reported vs. Li/Li$^+$.

density (2 mA cm$^{-2}$ in this case) can be rationalized on the basis of the mass transport of Li$^+$ ions from the electrode surface. Mass transport from sharp objects such as dendrites is enhanced leading to lower stripping overpotential and resulting in a plateau at lower potentials. If the lower and higher potential plateaus are attributed to Li stripping from rougher and smoother surfaces, respectively, a longer plateau at higher potential should lead to higher coulombic efficiency. Indeed, an excellent agreement is found as shown in Figure 8.

For 1 s plating pulses, the lowest coulombic efficiency was derived while no higher potential plateau was observed. As the duration of the plating pulses decreased, the coulombic efficiency increased and the duration of the higher potential plateaus increased. These results reveal that the trend in Li stripping overpotential can be used as a simple estimation of the roughening of the electrode surface, which is of key importance for efficient Li plating. In this case, higher overpotentials are beneficial since this will indicate planar diffusion to smooth Li electrode surface.

Figure 8b shows the evolution of the coulombic efficiency as a function of the duration of the relaxation pulses at a constant duration of plating pulses (0.125 s). The efficiency dropped when the duration of the relaxation pulses was reduced from 0.5 s to 0.25 s. It is necessary to apply relaxation pulses longer than 0.25 s for effective replenishment of the concentration of Li$^+$ ions at the electrode surface. As for the potential profiles, the most efficient plating conditions resulted in a larger plateau at higher potentials. Interestingly, the coulombic efficiencies for relaxation pulses of 0.250 s and 0.125 s were very similar, while the length of the plateau at higher overpotentials was slightly higher for 0.250 s. Actually, the results from the length of the plateau are more consistent with the theoretically expected trend since longer duration of the relaxation pulses is supposed to be beneficial. It should be noted that fine roughness analysis by e.g. AFM is prevented by interferences from the SEI formed on top of the Li film.

With this exemplary case, we aim to demonstrate the potential of the SDC as reliable and accelerating technique in Li batteries research. Figure 7 shows that the relative error is below 1.2%. Figure 7 contains results from 30 individual experiments, which required approximate 1 h since the SDC conducted autonomously all measurements. As assembling, disassembling and cleaning of a cell inside an Ar-filled glovebox takes at least 2 h, performing 30 experiments would have taken at least 60 h. Considering the movement range of the stepper motors of the SDC (12 mm in x- and 25 mm in y-direction) and a diameter of the tip of 0.5 mm, up to 300 experiments (1 mm$^2$ per spot) could be performed autonomously.

## 3. Conclusions

The technical details regarding the adaptation of the scanning droplet cell systems for non-aqueous battery research under complete exclusion of air (oxygen and water) and its application to optimize pulsed Li plating is shown. Efficient Li metal plating was investigated using the SDC system since the coulombic efficiency of this process is of prime importance for the development of high-energy Li metal batteries. The SDC provided several important findings namely that *i)* pulse charging protocols can effectively enhance the coulombic efficiency of Li plating at high current densities, and *ii)* the pulse protocol requires fine tuning of the parameters to be effective.

## Experimental Section

### Materials

The electrolyte was composed of 0.5 M $LiPF_6$ (Novolyte) dissolved in anhydrous propylene carbonate (Sigma Aldrich®, 99.7%). Metallic lithium was cut from a 0.38 mm thick ribbon (Sigma Aldrich®, 99.9%) from which the intrinsic and native passivation layer was mechanically removed. For fabrication of counter electrode (CE) and reference electrode (RE) lithium was pressed into a stainless steel canula (Sterican) sealed with solder tin. 2 mm diameter lithium discs were punched out from Li foil (Hoffmann hole punch) and attached to the CE steel tube. For the plating study on copper a photo positive epoxy board with a 1.5 mm thick copper coating (Bungard) was utilized. After complete removal of the protection foil using 2-propanol, the board was immediately introduced into the glovebox to minimize the formation of copper oxide.

### Automatized SDC setup

The SDC cell body was mounted on a force sensor, whose force values served as a feedback signal to stop the approach of SDC tip to the substrate surface. The force limits were 500 mN for Cu and 50 mN for Li. The opening diameters of the Teflon SDC tips were 1 mm for the copper substrates and 0.5 mm for lithium substrates due to their higher wettability by organic solvents. Prior to the measurements, the SDC tips were polished on a lapping film (3 M TM 266X, 3 Micron). Before approaching to a new measurement spot, 300 µl of fresh electrolyte was pumped into the cell with a Tecan Cavro XC syringe pump.

### Electrochemical measurements

All electrochemical measurements were conducted with a scanning droplet cell (SDC) setup in an Ar-filled glovebox. Potentiostatic and galvanostatic techniques were carried out with a µ-AutolabIII/FRA2 potentiostat and a BioLogic SP-300 potentiostat, respectively. In case of the galvanostatic Li plating/stripping tests on Cu the total charge for all plating procedures was fixed at 0.167 $mA\,h\,cm^{-2}$. The subsequent stripping of Li was stopped once the cut-off potential of $+1$ V vs. $Li/Li^+$ was reached. The standard pulse profile had a pulse duration of 2 s with 1 s of relaxation time at $-1$ nA between each pulse. Prior to the Li electrochemistry, a SEI layer was formed potentiostatically on Cu ($+0.05$ V vs $Li/Li^+$) to prevent mixed deposition with electrolyte species.

### Morphological characterization by SEM

Before morphological studies, all samples were shortly immersed in diethyl carbonate in order to remove electrolyte residues. A Quanta 3D FEG scanning electron microscope was operated at an acceleration voltage of 20 kV under high-vacuum conditions ($< 6\,E^{-4}$ Pa). Short transportation pathways between glovebox and SEM guaranteed a short sample exposure time ($< 30$ s) to oxygen and moisture.

## Acknowledgements

*E.V. acknowledges the financial support by the Spanish Government (MINECO) through the Research Challenges Programme (Grant RTI2018-099228-A-I00) and Ramón y Cajal award (RYC2018-026086-I) as well as the NanoBat project. NanoBat has received funding from the European Union's Horizon 2020 research and innovation programme under Grant Agreement no. 861962. Open access funding enabled and organized by Projekt DEAL.*

## Conflict of Interest

The authors declare no conflict of interest.

**Keywords:** Li metal · Li plating · automatization · scanning electrochemical technique · high-throughput

[1] M. A. Hannan, M. M. Hoque, A. Mohamed, A. Ayob, *Renewable Sustainable Energy Rev.* **2017**, *69*, 771.
[2] L. Trahey, F. R. Brushett, N. P. Balsara, G. Ceder, L. Cheng, Y.-M. Chiang, N. T. Hahn, B. J. Ingram, S. D. Minteer, J. S. Moore et al., *Proc. Natl. Acad. Sci. USA* **2020**, *117*, 12550.
[3] M. S. Whittingham, *Proc. IEEE* **2012**, *100*, 1518.
[4] F. Duffner, N. Kronemeyer, J. Tübke, J. Leker, M. Winter, R. Schmuch, *Nat. Energy* **2021**, *6*, 123.
[5] B. Dunn, H. Kamath, J.-M. Tarascon, *Science* **2011**, *334*, 928.
[6] Y. Shen, Y. Zhang, S. Han, J. Wang, Z. Peng, L. Chen, *Joule* **2018**, *2*, 1674.
[7] T. Liu, J. P. Vivek, E. W. Zhao, J. Lei, N. Garcia-Araez, C. P. Grey, *Chem. Rev.* **2020**, *120*, 6558.
[8] T. Li, X. Bai, U. Gulzar, Y.-J. Bai, C. Capiglia, W. Deng, X. Zhou, Z. Liu, Z. Feng, R. Proietti Zaccaria, *Adv. Funct. Mater.* **2019**, *29*, 1901730.
[9] Y.-K. Sun, *ACS Energy Lett.* **2020**, *5*, 3221.
[10] X. Shen, H. Liu, X.-B. Cheng, C. Yan, J.-Q. Huang, *Energy Storage Mater.* **2018**, *12*, 161.
[11] B. Scrosati, *J. Solid State Electrochem.* **2011**, *15*, 1623.
[12] D. Lin, Y. Liu, Y. Cui, *Nat. Nanotechnol.* **2017**, *12*, 194.
[13] W. Xu, J. Wang, F. Ding, X. Chen, E. Nasybulin, Y. Zhang, J.-G. Zhang, *Energy Environ. Sci.* **2014**, *7*, 513.
[14] R. Xu, X.-B. Cheng, C. Yan, X.-Q. Zhang, Y. Xiao, C.-Z. Zhao, J.-Q. Huang, Q. Zhang, *Matter* **2019**, *1*, 317.
[15] D. Rehnlund, C. Ihrfors, J. Maibach, L. Nyholm, *Mater. Today* **2018**, *21*, 1010.
[16] F. Ding, W. Xu, G. L. Graff, J. Zhang, M. L. Sushko, X. Chen, Y. Shao, M. H. Engelhard, Z. Nie, J. Xiao et al., *J. Am. Chem. Soc.* **2013**, *135*, 4450.
[17] N.-W. Li, Y.-X. Yin, C.-P. Yang, Y.-G. Guo, *Adv. Mater.* **2016**, *28*, 1853.
[18] G. Zheng, S. W. Lee, Z. Liang, H.-W. Lee, K. Yan, H. Yao, H. Wang, W. Li, S. Chu, Y. Cui, *Nat. Nanotechnol.* **2014**, *9*, 618.
[19] K. A. Lill, A. W. Hassel, G. Frommeyer, M. Stratmann, *Electrochim. Acta* **2005**, *51*, 978.
[20] J. M. Gregoire, C. Xiang, X. Liu, M. Marcin, J. Jin, *Rev. Sci. Instrum.* **2013**, *84*, 24102.
[21] J. P. Kollender, J. Gasiorowski, N. S. Sariciftci, A. I. Mardare, A. W. Hassel, *J. Phys. Chem. C* **2014**, *118*, 16919.
[22] S. Kumari, C. Khare, F. Xi, M. Nowak, K. Sliozberg, R. Gutkowski, P. S. Bassi, S. Fiechter, W. Schuhmann, A. Ludwig, *Z. Phys. Chem.* **2020**, *234*, 867.
[23] G. Garcia, E. Ventosa, W. Schuhmann, *ACS Appl. Mater. Interfaces* **2017**, *9*, 18691.
[24] M.-S. Wu, P.-C. J. Chiang, J.-C. Lin, *J. Electrochem. Soc.* **2005**, *152*, A47.
[25] J. R. Belt, D. M. Bernardi, V. Utgikar, *J. Electrochem. Soc.* **2014**, *161*, A1116-A1126.
[26] E. McTurk, C. R. Birkl, M. R. Roberts, D. A. Howey, P. G. Bruce, *ECS Electrochem. Lett.* **2015**, *4*, A145-A147.
[27] W. Zhou, S. Wang, Y. Li, S. Xin, A. Manthiram, J. B. Goodenough, *J. Am. Chem. Soc.* **2016**, *138*, 9385.
[28] J. L. Barton, *Proc. R. Soc. London Ser. A* **1962**, *268*, 485.
[29] H. Yang, E. O. Fey, B. D. Trimm, N. Dimitrov, M. S. Whittingham, *J. Power Sources* **2014**, *272*, 900.
[30] G. Bieker, M. Winter, P. Bieker, *Phys. Chem. Chem. Phys.* **2015**, *17*, 8670.

Manuscript received: May 29, 2021
Revised manuscript received: July 23, 2021
Accepted manuscript online: July 23, 2021